Acta Oceanol. Sin., 2024, Vol. 43, No. 2, P. 67–82
https://doi.org/10.1007/s13131-023-2262-y
http://www.aosocean.com
E-mail: ocean2@hyxb.org.cn

Diagenetic evolution and reservoir quality of the Oligocene sandstones in the Baiyun Sag, Pearl River Mouth Basin, South China Sea

Bing Tian[1]*, Shanshan Zuo[2], Youwei Zheng[1], Jie Zhang[1], Jiayu Du[1], Jun Tang[2]

[1] Institute of Mining and Coal, Inner Mongolia University of Science and Technology, Baotou 014010, China

[2] Institute of Science, Inner Mongolia University of Science and Technology, Baotou 014010, China

Received 6 June 2023; accepted 30 August 2023

Abstract

The Oligocene Zhuhai sandstones are significant reservoirs for hydrocarbons in the Baiyun Sag, South China Sea. For effective appraisal, exploration and exploitation of such a deep-water hydrocarbon sandstone, samples of five wells from depths of 850 m to 3 000 m were studied. A series of comprehensive petrographic and geochemical analyses were performed to unravel the diagenetic features and their impact on the reservoir quality. Petrographically, the sandstones are dominated by feldspathic litharenites and lithic arenites with fine to medium grain sizes and moderate to good sorting. The reservoir quality varies greatly with a range of porosity from 0.2% to 36.1% and permeability from 0.016 $\times 10^{-3}$ μm^2 to 4 301 $\times 10^{-3}$ μm^2, which is attributed to complex diagenetic evolution related to sedimentary facies; these include compaction, cementation of calcite, dolomite, siderite and framboidal pyrite in eogenetic stage; further compaction, feldspar dissolution, precipitation of ferrocalcite and ankerite, quartz cements, formation of kaolinite and its illitization, precipitation of albite and nodular pyrite, as well as hydrocarbon charge in mesogenetic stage. The dissolution of feldspar and illitization of kaolinite provide internal sources for the precipitation of quartz cement, while carbonate cements are derived from external sources related to interbedded mudstones and deep fluid. Compaction is the predominant factor in reducing the total porosity, followed by carbonate cementation that leads to strong heterogeneity. Feldspar dissolution and concomitant quartz and clay cementation barely changes the porosity but significantly reduces the permeability. The high-quality reservoirs can be concluded as medium-grained sandstones lying in the central parts of thick underwater distributary channel sandbodies (>2 m) with a high content of detrital quartz but low cement.

Key words: Baiyun Sag, Oligocene, Zhuhai Formation, diagenesis, reservoir quality

Citation: Tian Bing, Zuo Shanshan, Zheng Youwei, Zhang Jie, Du Jiayu, Tang Jun. 2024. Diagenetic evolution and reservoir quality of the Oligocene sandstones in the Baiyun Sag, Pearl River Mouth Basin, South China Sea. Acta Oceanologica Sinica, 43(2): 67–82, doi: 10.1007/s13131-023-2262-y

1 Introduction

Reservoir quality is one of the major uncertainties in hydrocarbon exploration and production (Bjørlykke, 2014; Pang et al., 2015; Muther et al., 2022). Porosity and permeability, the crucial petrophysical properties used for reservoir quality representation, are hardly predictable because they are dependent on both the original depositional environment and secondary diagenetic alterations (Bjørlykke and Jahren, 2012; Kassem et al., 2022). The depositional environment exerts profound influences on reservoir quality via determining lithology, geometry, and original porosity of the sediments, and further affects pore-fluid composition and diagenetic evolution during subsequent burial (Kassem et al., 2021; Shehata et al., 2021). Diagenesis consists of a range of complex physical and chemical reactions, such as compaction, cementation, and dissolution, which distinctly reshape the reservoir quality (Bjørlykke, 2014).

The Baiyun Sag is an important petroleum- and natural gas-bearing sag in the offshore area of China (Zhu et al., 2008; Mi et al., 2016). Breakthroughs have been made in deep-water hydrocarbons in the Oligocene Zhuhai Formation. The reservoir quality and heterogeneity of the Zhuhai sandstones have become a serious obstacle to finding additional reserves. To date, several studies have investigated the diagenetic events and reservoir features of the target reservoir (Lei et al., 2018; Li et al., 2021; Liao et al., 2022; Wen et al., 2022; Xie et al., 2022). In previous studies on the effects of diagenesis on the quality of the sandstone reservoirs, it has been argued that: (1) the dissolution of feldspar and igneous rock debris to enhance porosity during the burial process (Liao et al., 2022; Wen et al., 2022; Xie et al., 2022) and (2) carbonate cementation in the sandstone with materials supplied from dissolution of feldspar, transformation of clay minerals and deep fluids (Wang et al., 2010; Wang et al., 2017; Du et al., 2019). The present study provides some fresh insights on this issue.

The principal objectives of this study are to (1) clarify distinct processes and establish the evolution history of diagenesis; (2) identify sources and sinks of the complex diagenetic pore-fluids; and (3) assess controls of various diagenetic reactions on reservoir quality of the Zhuhai sandstones. A better understanding of these processes will facilitate further hydrocarbon explorations of the sandstone reservoirs in the study area and provide

Foundation item: The National Natural Science Foundation of China under contract No. 42262020; the Research Program of Science and Technology at Universities of Inner Mongolia Autonomous Region under contract No. NJZY22445.
*Corresponding author, E-mail: tb_imust@163.com

some theoretical basis for predictive models of multiple-layer sandstone reservoirs.

2 Geological setting

2.1 *Tectonics*

The Pearl River Mouth Basin is located in the northern slope of the South China Sea (SCS) (Fig. 1). The basin covers an area of 17.5×10^4 km^2 and has water depths of 200 m to 2 000 m (Li et al., 2021). Five first-order tectonic zones can be further identified (Fig. 1a). Tectonic evolution of the basin can be categorised into three major tectonic stages since the Cenozoic, which include extensional rifting (before about 30 Ma), transition (recording mid-ocean ridge spreading and developing of a breakup unconformity) (30–23.8 Ma), and thermal subsidence (23.8 Ma–present). The basin was in an extension environment, with multiperiod structural movements including the Shenhu movement, the Zhuqiong movement, Nanhai movement, Baiyun movement, and Dongsha movement (Fig. 2) (Zhou et al., 2015; Morley, 2016). The study area, which is one of the most deep-water hydrocarbon-rich areas in the basin, lies in the southeast of Baiyun Sag (Fig. 1b).

2.2 *Stratigraphic framework*

In an ascending order, Cenozoic sedimentary sequences in the Baiyun Sag consist of a syn-rift continental sequence comprising the Paleogene Shenhu, Wenchang and Enping formations, and a post-rift marine sequence including the Oligocene Zhuhai Formation, the Neogene, and the Quaternary groups (Fig. 2) (Pang et al., 2008). The studied section, i.e., the Zhuhai Formation, is composed of multi-stage, shelf-margin delta of medium- to-fine sandstones close to the shelf break interbedded with dark marine mudstones, calcareous mudstones and subordinate carbonates (Fig. 2).

2.3 *Depositional setting*

The Nanhai movement (ca. 32 Ma) marked the end of the rifting stage and the start of the seafloor spreading of the northern SCS. The basin was featured by broad continental shelf and narrow continental slope in this fault-depression transition stage (Morley, 2016). At the onset of Zhuhai interval deposition, large scale of transgression occurred in Baiyun Sag, and consequently, extensive littoral-neritic facies developed. During much of the Zhuhai deposition, the Paleo-Pearl (Zhujiang) River transported abundant terrigenous clasts into the sea, and a large river-delta system was widely distributed on the broad continental shelf of the northern SCS (Mansurbeg et al., 2008; Morley, 2016). The study area is located downstream of the river-delta system of the Paleo-Pearl River. Due to the abundant supply, siliciclastic sediments prograded to and passed across the shelf break and formed thick clinoforms in the shelf margin area, giving rise to a typical shelf-margin delta system.

3 Datasets and methods

The study interval, the Zhuhai Formation, has been a number of offshore oil and gas fields drilling target layer in the southeastern Baiyun Sag. Therefore, plenty of core material and other data can be obtained for this research. Petrographic data of 90 thin sections, 145 reservoir porosity and permeability testing results, 116 grain-size analysis data, and 56 bulk rock X-ray diffraction (XRD) data of five wells (LW1-1, LW1-2, LW2-1, LW3-1, LW4-1 in Fig. 1b) were collected from CNOOC Research Institute Co., Ltd.

According to the study objectives and data accessibility, 65 samples of core and cuttings were selected from the five wells mentioned above and from various depositional facies and span a wide degree of diagenesis. The sedimentary and stratigraphic characteristics of the Zhuhai sandstones were interpreted from core data.

Routine rock properties (porosity and permeability) were tested on all samples using a 3 020-62 helium porosity analyzer and GDS-9F gas permeability analyzer at common temperature and humidity.

Sixty-five impregnated thin sections were prepared for mineralogical composition, textural framework, and visual porosity characterization. Moreover, 26 thin sections of them were stained

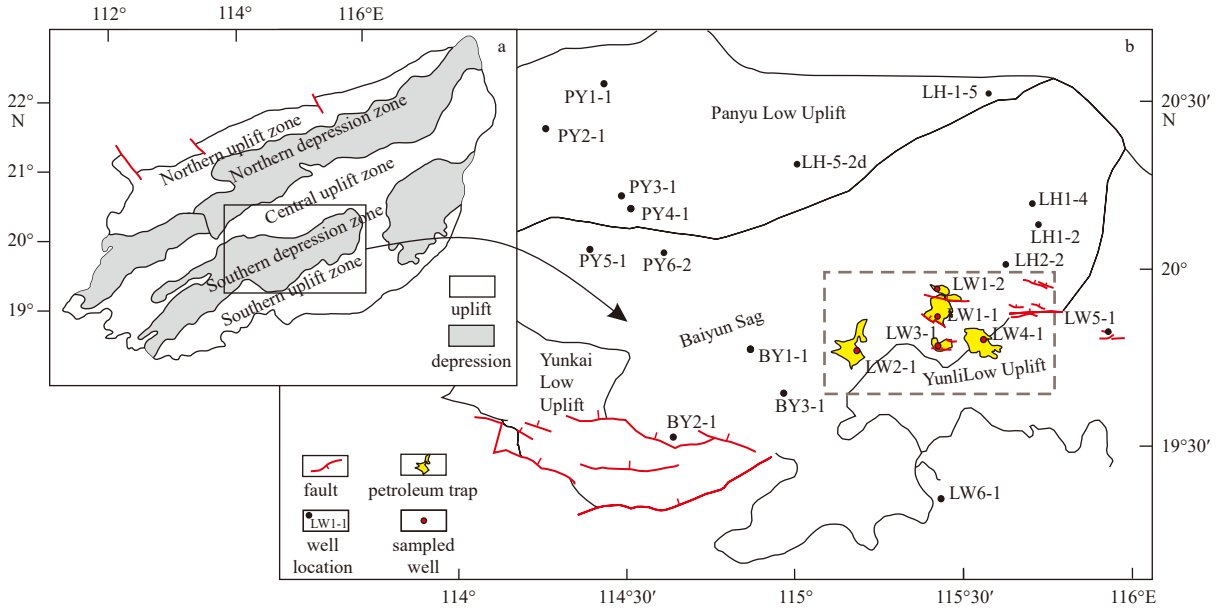

Fig. 1. Locality map of tectonic zones of the Pearl River Mouth Basin, SCS (modified from Lei et al., 2018) (a). Map of well locations referred to in the article in the southeastern Baiyun Sag (b).

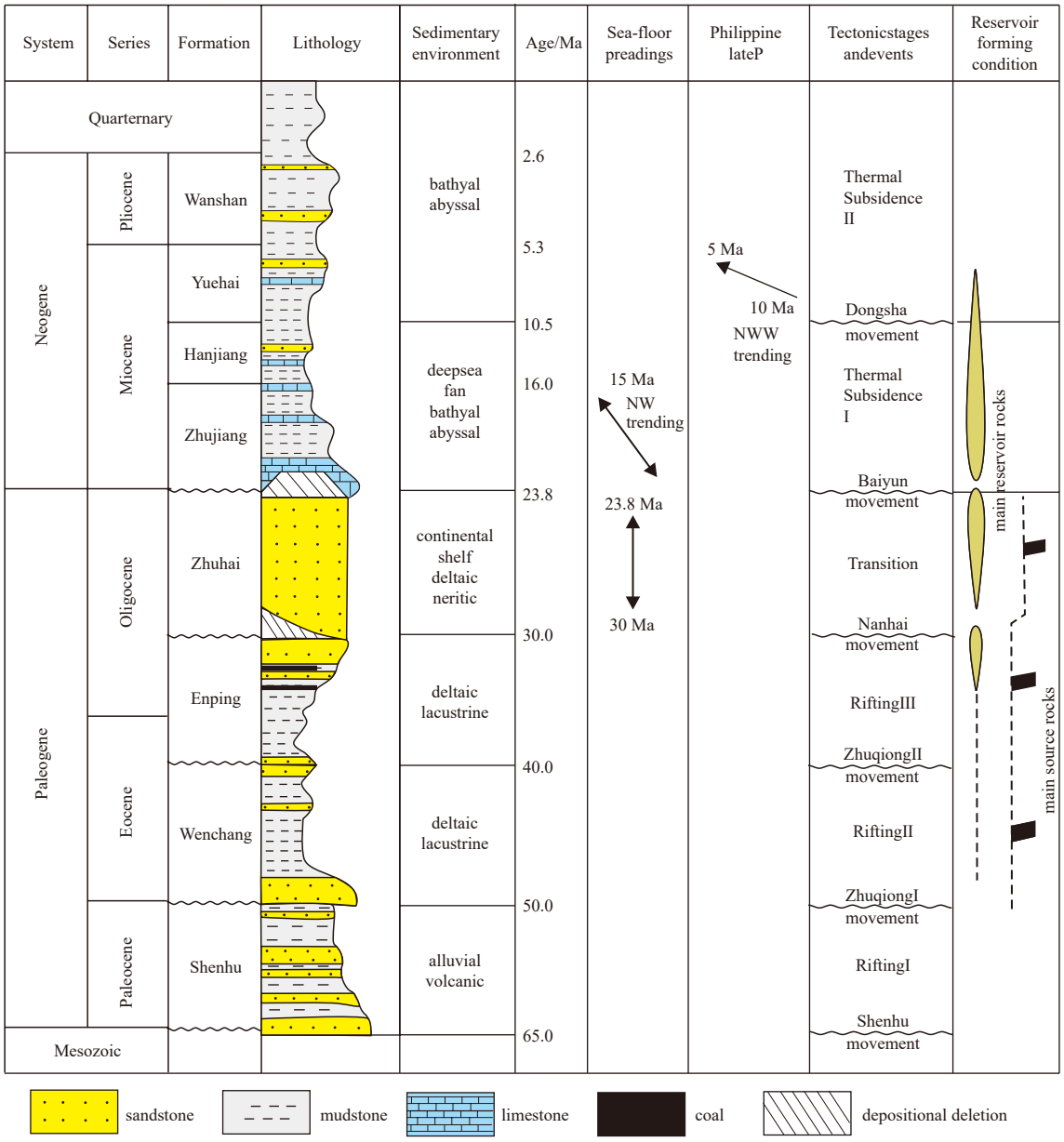

Fig. 2. Cenozoic-Quaternary tectonic, stratigraphic and sedimentary evolution of the Baiyun Sag (modified from Lei et al., 2018).

with Alizarin Red S for carbonate cement characterization. Point-count was performed on all samples to estimate the modal composition. Three hundred points were counted per thin section (Stroker et al., 2013). The values and types of pore spaces were also counted during point counting in the thin-section analyses. Petrographic analysis and visual porosity were found out through Zeiss microscope and AxioVision software Rel.

To confirm the petrographic characterization, all samples were prepared using an Ultima IV X-ray diffractometer. XRD analysis was based on the procedure used by Moore and Reynolds (1997) and Mangi et al. (2022) within an error range of 10%. In addition, for the spatial morphology of authigenic minerals identification, 22 gold-coated samples were observed under a ZEISS EVO LS15 scanning electron microscope (SEM).

After detailed petrographic desscription of thin-sections, seven core samples were prepared as doubly polished fluid-inclusion wafers for microthermometric measurement. Microthermometry was conducted using a calibrated LINKAM THMSG600 stage. The homogenization temperature (Th) was obtained by cycling. The Th value measured precision was ±1℃.

For carbon and oxygen isotope measurements, 30 organic matter-free samples were prepared. The carbon and oxygen stable isotope values were obtained from CO_2 liberated from carbonate cement samples using Thermo-Finnigan MAT 253 IRMS. The measurement precision was ±0.014‰ for oxygen and ±0.020‰ for carbon. The stable isotope data were reported in δ notation relative to PEE Dee belemnite (V-PDB). $\delta^{18}O_{VPDB}$ values were converted to $\delta^{18}O_{VSMOW}$ (Vienna standard mean ocean water) values using the equation of Coplen et al. (1983). All the analyses mentioned above were done in the Key Laboratory of Petroleum Resources Research, Chinese Academy of Sciences (Lanzhou).

4 Results

4.1 *Sedimentary micro-facies*

Of the various shelf-margin delta facies recognized in the core

descriptions, the most common are the subaqueous distributary channel micro-facies (Tian et al., 2022). These sandstones are composed of fine to medium-grained, fining upwards, and several meters in thickness with massive bedding and wedge cross bedding (Fig. 3a). In the vertical profile, they often change into siltstones and pinch-out into mudstones.

The most striking feature of mouth bar sandstones is the higher quartz content, lower matrix content and better sorting. This can be attributed to the frequent water washing and relatively high sedimentation rate of this micro-facies (Tian et al., 2022). Due to the decrease in water energy, the mouth bar sandstones are finer in particle size than those of the subaqueous distributary channel. Coarser upwards in the profile, parallel bedding and sediment deformation are typically observed in mouth bar sandbodies (Fig. 3b), which are significantly different from the subaqueous distributary channel sandbodies.

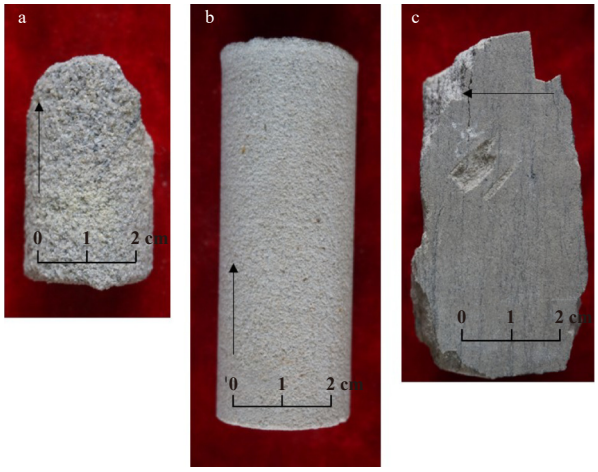

Fig. 3. Core photos showing the lithofacies characteristics of the Zhuhai sandstones. a. LW1-1, 2 037.5 m, grey medium-grained sandstones with massive bedding; b. LW1-1, 2 027.25 m, grey fine-grained sandstones with parallel bedding; c. LW1-1, 2 563.5 m, grey-black mudstones and siltstones with horizontal bedding. The black arrow shows the upward direction of the formation.

The distributary bay and marine micro-facies are characterized by a typically low-energy sedimentary environment, and dominated by the finest sediments, mainly mudstones and siltstones (Fig. 3c) (Tian et al., 2022).

4.2 *Sandstone petrology: detrital mineralogy*

Based on point-count data, the studied Zhuhai sandstones are mainly feldspathic litharenites followed by lithic arkoses according to terminology of Folk (1968) (Fig. 4a). Detrital quartz grains account for 34%–85% (average 56.5%). The detrital feldspar content ranges from 3% to 38.5% (average 20.3%), and the content of K-feldspar (14.9%) is higher than plagioclase (5.4%). The rock fragments account for 4%–38.2% (average 23.2%), and are composed of volcanic rock fragments (average 13.8%), sedimentary rock fragments (average 2.78%), and metamorphic rock fragments (average 6.62%). Only small quantities of micas and heavy minerals can be found. The mud content is 0.3%–45% (average 4.68%), and the cement content is 0.2%–32.3% (average 7.24%). The compositional maturity is 1.55 (ranges from 0.52 to 5.67).

The sandstones are mostly fine-grained to medium-grained (Fig. 4b). The detrital grains are moderate to well sorted (Fig. 4c), with subangular to sub-rounded grain shape. Point to line contacts is most common between detrital grains, followed by few concavo-convex contacts.

4.3 *Sandstone petrology: diagenetic mineralogy*

The diagenetic alterations recognized in the Zhuhai sandstones are compaction, cementation (carbonates, quartz, and clay minerals), and dissolution of feldspar grains. Carbonates, authigenic quartz, clays (authigenic and detrital), pyrites and albite are the major pore-filling constituents.

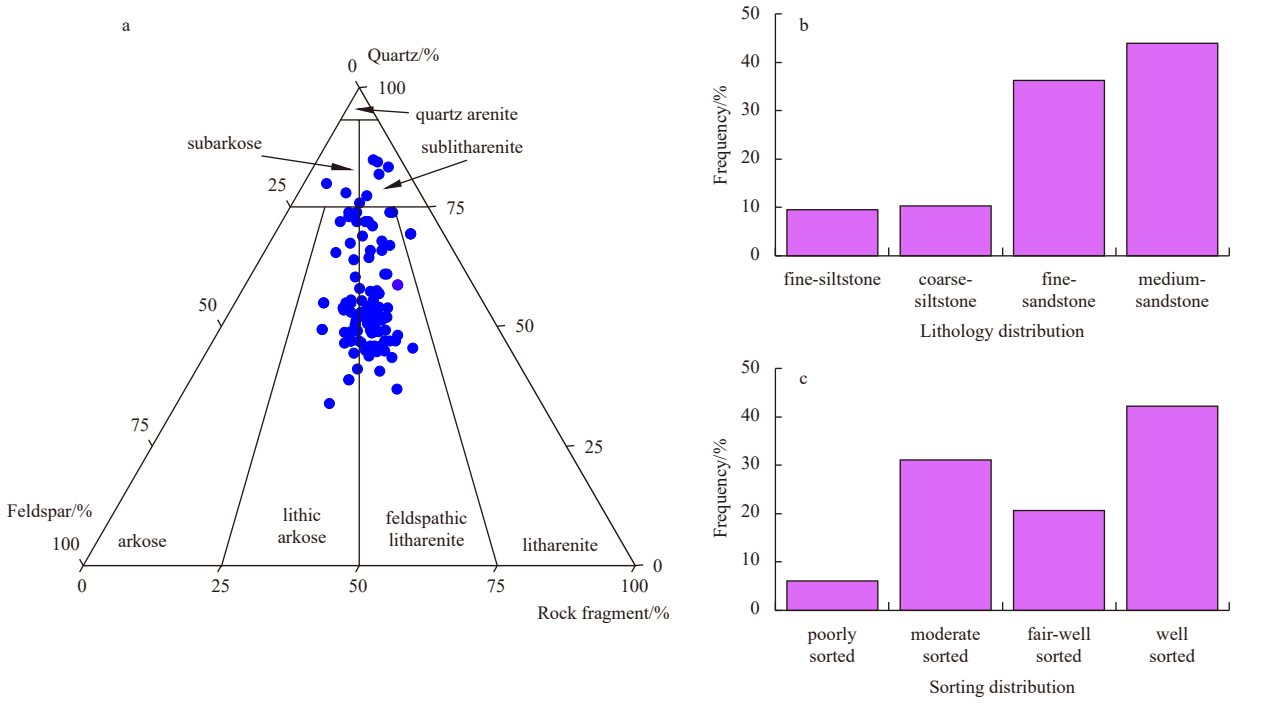

Fig. 4. Reservoir lithologic characteristics of the Zhuhai sandstone. a. Classification of sandstone; b. Lithology distribution; c. Sorting distribution.

4.3.1 *Carbonate cements*

Carbonate cement is the dominant type of diagenetic mineral and volumetrically ranges from 0.2% to 28%. Five types of carbonate cements are recognized in the studied sandstones, which are calcite, dolomite, ferrocalcite, ankerite, and siderite (Figs 5a–f). Calcite (0.1%–20.3%, average 2.54%) mainly presents as pore-filling poikilotopic blocky crystals varying from 5 μm to 300 μm in size, which infill primary pores or replace detrital grains.

Calcite cemented tight sandstone (12.5%–20.3%) typically occurs at the edge of the sandstone bed (Fig. 5a). Calcite was observed to be engulfed by ferroan calcite (Fig. 5b).

Dolomite (0.2%–8.7%, average 1.07%) commonly composed of microsparry or micritic aggregates (5–250 μm) generally appears as rhombohedral crystals (Figs 5c–d). Dolomite cements were also observed to fill primary pores between uncompacted framework grains as poikilotopic and pore-filling cement. Dolomite is less abundant than calcite.

Ferroan calcite (0.2%–7.6%, average 1.69%) commonly occurs as scattered euhedral or isolated crystals (15–200 μm; Fig. 5b), ankerite (0.3%–24.3%, average 4.62%) mostly occurs as mosaic clusters (10–250 μm; Fig. 5d) and euhedral rhombs (10–150 μm; Fig. 5e). These cements mainly occur as pore fillings and partly occupy pores caused by fracture and feldspar dissolution (Figs 5e–f), and replace early cements or framework grains (Figs 5b–d). The color of siderite ranges from light to dark brown. It appears in the form of irregular ankerite rhombs and typically fills primary pores (Fig. 5f). There are extensive carbonate cements (9%–28.8% in content, average 16.85%) in sandstones within 1.0 m of the sandstone-mudstone contact, and they decrease sharply to the central part of sandstone beds (1.5%–14.8% in content, average 7.54%). This indicates that the further the distance to the contact, the less the carbonate cement in sandstone (Fig. 6a).

4.3.2 *Feldspar dissolution*

Partial to complete feldspar grain dissolving is widespread in the Zhuhai interval. The dissolution process can be demonstrated by the common irregular dissolution edge and feldspar residue (Figs 5g–i). Feldspar grains dissolved preferentially along the cleavages (Fig. 5g), and some of them were almost totally dissolved, forming moldic pores (Figs 5h–i). Noting that feldspar dissolution pores always bring with the pore-filling authigenic clay and quartz cements (Figs 5h–i). The mean abundance of feldspar dissolution porosity is 1.26% (range 0.1% to 3.1%). The closer the distance to the contact, the less feldspar dissolution pores in sandstone (Fig. 6b).

4.3.3 *Quartz cements*

Quartz cements make up less than 1% (Fig. 6c) and commonly appear as syntaxial overgrowths (Figs 7a–b) and some small prismatic euhedral crystals (Fig. 7a). The presence of a dust clay ring makes it easy to distinguish quartz overgrowths from detrital grains (Figs 5d–e). Locally, there are two phases of quartz overgrowth (Fig. 7b) with thicknesses varying from 2 μm to 60

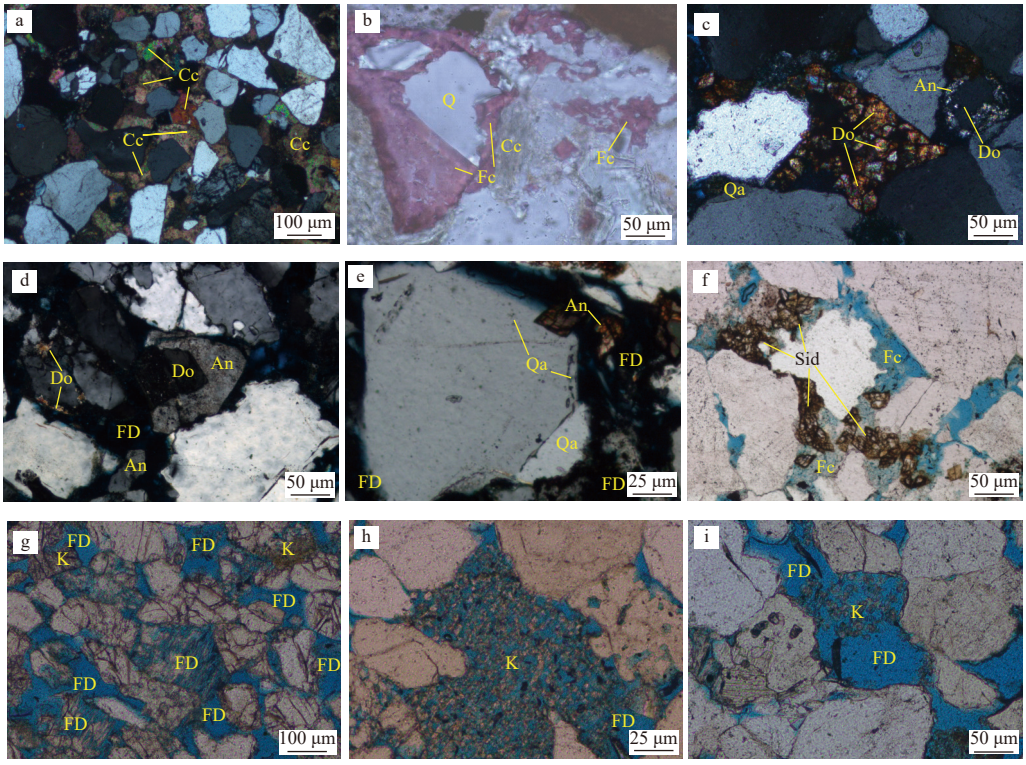

Fig. 5. Photomicrographs of diagenetic minerals. a. LW1-1, 2 027.25 m, poikilotopic, locky calcite filled most primary pores. b. LW1-2, 2 563.5 m, calcite was replaced by ferrocalcite. c. LW1-1, 2 037.5 m, dolomite filled intergranular primary pores, dolomite zoned and engulfed by ankerite. d. LW1-2, 2 563.5 m, feldspar secondary pores and partly filled by some ankerite, quartz overgrowths were replaced by ankerite. e. LW1-1, 2 037.5 m, dolomite was engulfed by ankerite. f. LW3-1, 1 861.5 m, siderite grains precipitated around the detrital grains. g. LW1-1, 1 707.5 m, feldspar secondary pores and partly filled by kaolinite, h. LW4-1, 1 519.8 m, micropores in authigenic kaolinite. i. LW1-2, 2 429.5 m, extensive feldspar dissolution partly filled by kaolinite with no dissolution of detrital carbonate grains. Cc = calcite; Do = dolomite; Q = quartz grain; Fc = ferroan calcite; An = ankerite; FD = feldspar dissolution pore; K = kaolinite; Qa = quartz overgrowths; Sid = siderite.

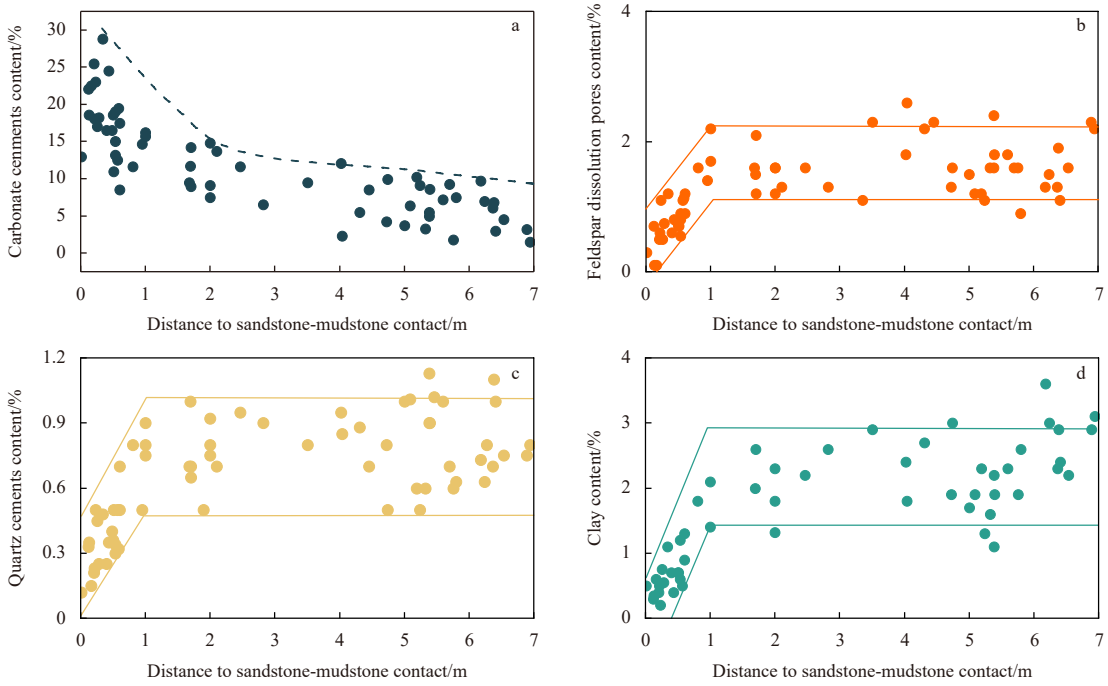

Fig. 6. The variation of the content of diagenetic products with the distance to sandstone–mudstone contact.

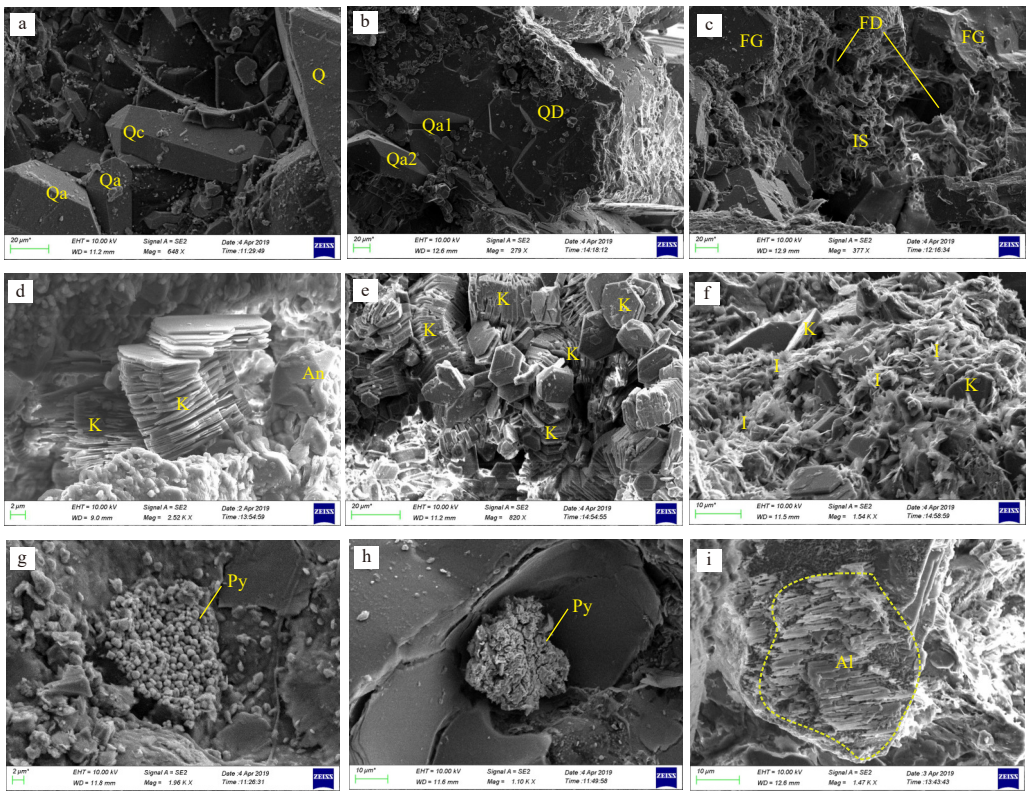

Fig. 7. SEM images of diagenetic minerals. a. LW1-1, 1 714.25 m, quartz overgrowths and prismatic quartz crystals. b. LW1-1, 2 563.5 m, two phases of quartz overgrowths. c. LW3-1, 1 861.5 m, feldspar secondary pores and IS. d. LW4-1, 1 559.8 m, kaolinite and ankerite in sandstones. e. LW3-1, 1 861.5 m, authigenic kaolinite in primary pores. f. LW1-2, 2 509.5 m, transition of kaolinite to illite. g. LW1-1, 1 655 m, spherical aggregates of micron-sized pyrite crystals. h. LW1-1, 2 563.5 m, irregular pore-filling pyrites in sandstones. i. LW1-2, 2 509.5 m, kaolinite and ankerite in sandstones. FG = feldspar grain, I = illite, Qa1 and Qa2 = two phases of quartz overgrowths, Qc = quartz crystals, Py = pyrite, Al = albite.

μm. The first stage of quartz overgrowth (Qa1) is enclosed or engulfed by ankerite and ferroan calcite cements (Figs 5d–e), indicating that ankerite and ferroan calcite cementation occurred after Qa1. As in the case of the feldspar secondary pores, the marginal

sandstones usually contain fewer quartz cements (0–0.7%) than the central sandstones in thick beds (0.5%–1.13%) (Fig. 6c).

4.3.4 *Clay minerals*

The authigenic clay minerals are kaolinite and illite in the studied interval, follow by illite/smectite mixed layer (I/S) and chlorite. The honeycomb-textured I/S occurs as schistose crystals, usually present with a curly margin of length 5–10 μm (Fig. 7c). Kaolinite occurs as euhedral booklets and vermicular pseudohexagonal aggregates, and is usually observed in feldspar secondary pores (Figs 5h–i). Significant intercrystalline microporosity can be identified from kaolinite aggregates (Fig. 7d). Kaolinite aggregates consist primarily of thin, closely associated platelets (Figs 7d–e). Some kaolinite crystals appear as fibrous edges due to illitization (Fig. 7e). Fibrous and flaky illite can also be observed in primary pores and feldspar secondary pores, with some located on grain surfaces (Fig. 7f). The total content of authigenic clay in the marginal part (0.2%–1.8%) is usually fewer than that in the central part of sandstone beds (1.3%–3.6%) (Fig. 6d).

XRD data of the clay fraction (<2 μm) of sandstones show that kaolinite is the major clay mineral and dominates when the depth is less than 2 000 m, and had a sharp fall below this depth, particularly, below about 2 500 m (Fig. 8a). Illite dominates with depth more than 2 000 m (Fig. 8b), which can also be verified by the photomicrograph (Figs 7c–f). The contents of I/S and chlorite exhibit an increasing trend within the depths of 1 900–2 100 m and 2 250–2 350 m, respectively (Figs 8c–d). The content of smectite in I/S obviously reduces below about 1 500 m (Fig. 8e).

4.3.5 *Accessory minerals*

Pyrite and albite can be identified as accessory diagenetic minerals with small content of less than 1%. In the Zhuhai sandstones, diagenetic pyrite occurs primarily as spherical aggregates of micron-sized pyrite crystals (1–30 μm), namely in the form of framboidal pyrite (Fig. 7g). In addition, parts of pyrite forms in irregular pore-filling nodular crystals, with some having replaced the ferroan calcite (Fig. 7h). The authigenic albite occurs as columnar aggregates of euhedral crystals, and the elongate euhedral crystals have a parallel orientation to the cleavages of dissolved K-feldspar (Fig. 7i).

4.4 *Reservoir properties*

4.4.1 *Porosity and permeability*

The porosity of the Zhuhai sandstones has a wide range between 0.2% and 36.1% and averages 21.74%. The permeability ranges from 0.016 $\times10^{-3}$ μm^2 to 4 301 $\times10^{-3}$ μm^2 and has an average of 721.28 $\times10^{-3}$ μm^2. On the whole, both of them decrease with increasing depth (Li et al., 2021). The decrease in the porosity is modest while the permeability falls sharply, and little evidence of anomalously high porosity exists (Figs 9a–b) (Lei et al., 2018). Similarly, in thin sections, the relative content of total visual porosity also decreases gradually as the burial depth increases from 850 m to 3 000 m (Fig. 9c), and the average percentage of feldspar dissolution pores shows an increasing trend from about 1.0% to 1.5% (Fig. 9d).

4.4.2 *Pore types*

Based on petrographic and SEM observations, total visual porosity in the Zhuhai Formation varies from 0.5% to 23.6% with an average of 10.03%, which can be divided into two main types: primary and secondary porosity.

Primary porosity represents a more significant percentage of the total pores (15.4%–98%, average 84.6%), and mainly consists of residual intergranular pores that show irregular polygons. They are formed when the original pores are filled with calcite, quartz, kaolinite, chlorite, etc. during diagenesis (Figs 5a–f).

Dissolution pores and intercrystal pores are the main secondary porosity types that can be commonly observed in the Zhuhai Formation. Dissolution pores consist of intergranular dissolution pores and intragranular dissolution pores (Figs 5g–i). They are mainly formed by dissolution of feldspar and volcanic rock debris (Figs 5g–i), ranging from 0.1% to 3.1%, with an average of 1.0%. Intercrystalline pores occur as micropores (0.5–6.5 μm in size) within authigenic kaolinite, chlorite and illite (Figs 7d–f).

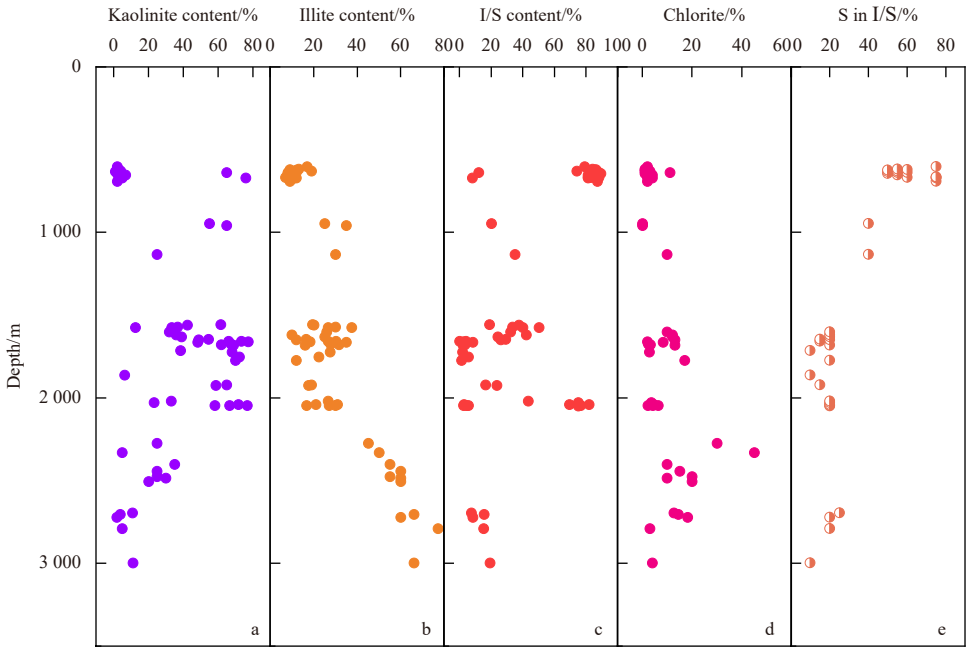

Fig. 8. Vertical distribution characteristics of clay cements. I/S = illite/smectite mixed layer; S: smectite.

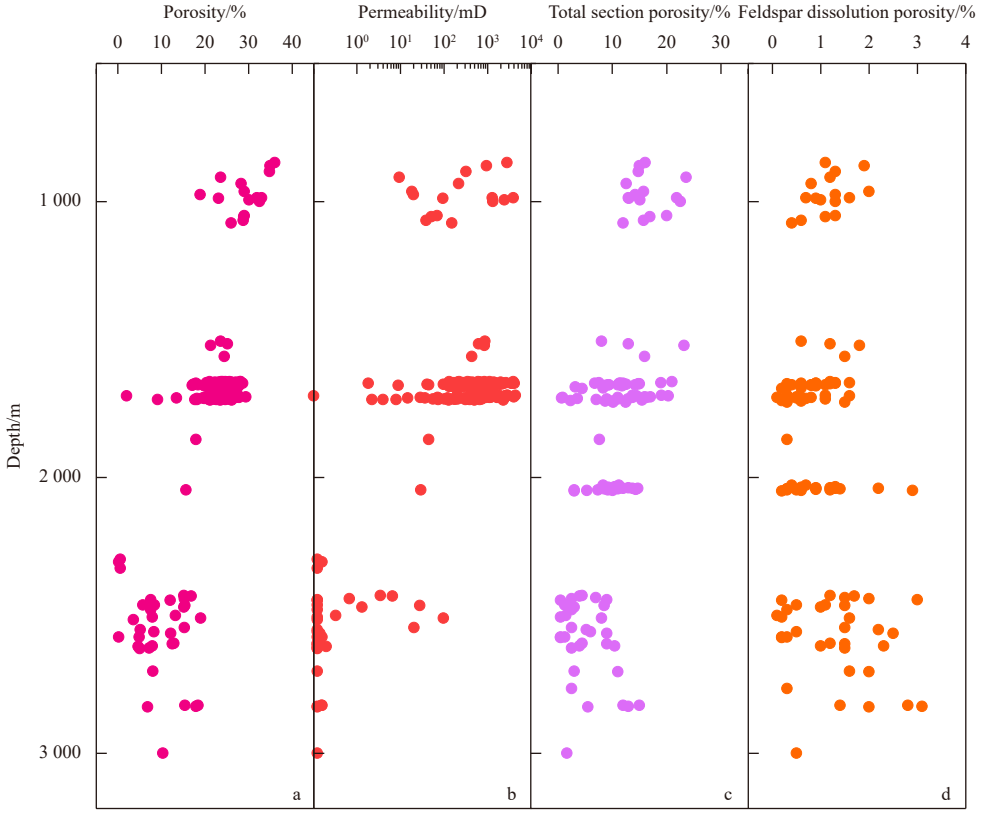

Fig. 9. Vertical distribution of porosity (a), permeability (b), total thin section porosity (c), and feldspar dissolution porosity (d).

4.5 *Mineral chemistry*

4.5.1 *Fluid inclusions*

The homogenization temperature (Th) of fluid inclusions is useful to represent the precipitation temperature of host minerals. Fluid inclusions are primarily present in the microfractures in detrital quartz (Fig. 10a), with some in the quartz overgrowths (Fig. 10b) and few in carbonate cements. At room temperature, they are commonly liquid-vapor two-phase inclusions with a diameter range of largely from 3 μm to 9.5 μm.

As shown in Table 1 and Fig. 11, the Th of fluid inclusions is between 77.5℃ and 125℃ in the quartz overgrowths, and from 94.3℃ to 146℃ in the microfractures in detrital quartz. Only two Th values are measured in ankerite, which are 113.7℃ and 124.3℃. Specifically, the mean Th value of fluid inclusions is 89.8℃ in Qa1 (varies from 77.5℃ to 107.9℃), and is 114.3℃ in Qa2 (from 104.5℃ to 125℃) (Table 1).

4.5.2 *Stable isotopic composition*

Figure 12 and Table 2 present the C and O isotopic data on carbonate cements. In specific, calcite cements have $\delta^{13}C_{VPDB}$ values between –0.3‰ and +2.51‰ and $\delta^{18}O_{VPDB}$ values ranging from –11.27‰ to –8.28‰. Similarly, $\delta^{13}C_{VPDB}$ values range from –0.76 ‰ to +2.12 ‰ and $\delta^{18}O_{VPDB}$ values are –11.24‰ to –8.49‰ in dolomite cements. $\delta^{13}C_{VPDB}$ values show significantly light for ferroan calcite cements, which are from –24.42‰ to –4.19‰ while $\delta^{18}O_{VPDB}$ values are slightly light and range from –16.63‰ to –13.67‰. $\delta^{13}C_{VPDB}$ values (–7.72‰ to –1.02 ‰) are significantly higher in ankerite cements without big changes in $\delta^{18}O_{VPDB}$ values (–18.05‰ to –12.06‰) as compared with ferroan calcite.

5 Discussion

5.1 *Paragenetic sequence of diagenesis*

According to Morad et al. (1990), diagenetic events can be

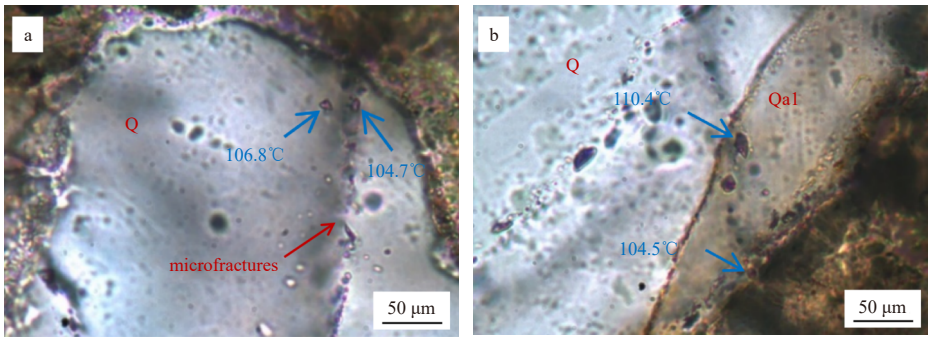

Fig. 10. Photomicrographs illustrating fluid inclusions in the Zhuhai sandstones. a. LW1-1, 1 663.54 m, fluid inclusions along healed microfractures in quartz grain, b. LW1-1, 2 045 m, fluid inclusions in quartz overgrowths.

Table 1. The homogenization temperature (Th) of fluid inclusions. Qa1 and Qa2 = two phases of quartz overgrowths; MF = microfractures; An = ankerite

Well	Depth/ m	Inclusion location	Size/μm	Th/℃	Well	Depth/m	Inclusion location	Size/μm	Th/℃
LW1-1	1 663.54	Qa1	5.2	83.2	LW1-1	2 045.0	MF	5.5	127.0
LW1-1	1 663.54	Qa1	6.2	77.5	LW1-1	2 045.0	MF	4.8	130.4
LW1-1	1 663.54	Qa1	7.0	95.3	LW1-2	2 609.1	Qa1	7.5	107.9
LW1-1	1 663.54	MF	6.7	95.7	LW1-2	2 609.1	MF	4.0	126.5
LW1-1	1 663.54	MF	8.0	97.9	LW1-2	2 609.1	MF	3.8	137.3
LW1-1	1 663.54	MF	4.5	104.7	LW1-2	2 609.1	MF	3.0	145.2
LW1-1	1 663.54	MF	5.7	106.8	LW1-2	2 702.5	Qa2	3.6	125.0
LW1-1	1 708.25	Qa1	4.7	84.5	LW1-2	2 702.5	Qa2	6.0	117.3
LW1-1	1 708.25	Qa1	8.5	90.4	LW1-2	2 702.5	MF	5.5	141.0
LW1-1	1 708.25	MF	8	94.3	LW1-2	2 702.5	MF	4.7	146.0
LW1-1	1 708.25	MF	3.5	97.5	LW1-2	2 702.5	MF	8.8	129.0
LW1-1	1 708.25	MF	7.0	106.7	Lw3-1	1 861.5	MF	4.8	112.3
LW1-1	1 708.25	MF	7.5	114.8	Lw3-1	1 861.5	MF	3.3	113.8
LW1-1	1 708.25	MF	5.0	111.3	Lw3-1	1 861.5	MF	9.5	117.1
LW1-1	1 708.25	MF	5.5	108.2	Lw3-1	1 861.5	MF	5.9	115.3
LW1-1	2 045.0	Qa1	5.9	89.5	Lw3-1	1 861.5	MF	7.1	120.1
LW1-1	2 045.0	Qa2	5.4	104.5	Lw3-1	1 861.5	MF	6.2	124.6
LW1-1	2 045.0	Qa2	7.0	110.4	LW1-2	2 702.5	An	5.5	113.7
LW1-1	2 045.0	MF	3.3	119.3	LW1-2	2 702.5	An	8.0	124.3
LW1-1	2 045.0	MF	7.1	124.2					

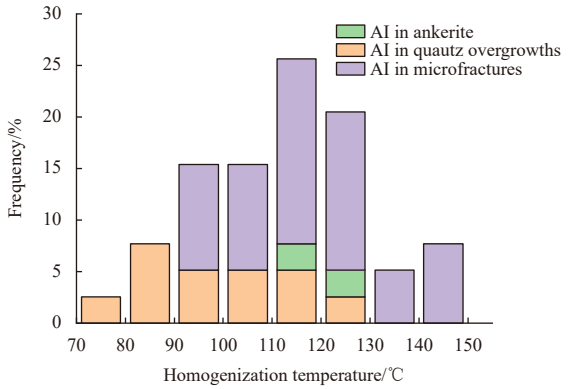

Fig. 11. Histograms of Th for fluid inclusions. Al = fluid inclusions.

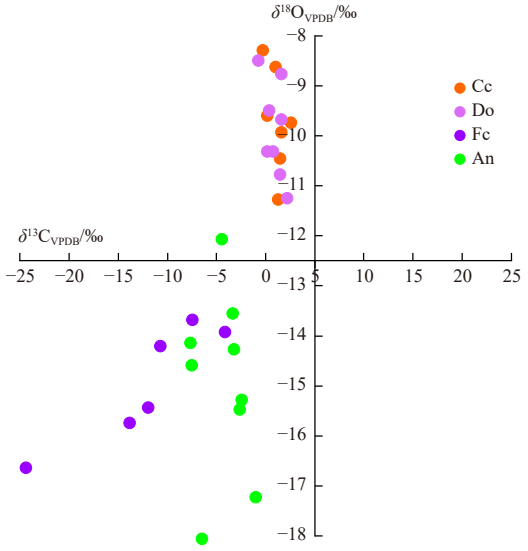

Fig. 12. Crossplot of Carbon and Oxygen isotopic compositions of carbonate cements. Cc = calcite; Do = dolomite; Fc = ferroan calcite; An = ankerite.

classified into two regimes: eogenesis (typically occurs at temperatures < 70℃ and at burial depth < 2 km during which pore-water is dominanted by depositional and/or meteoric waters) and mesogenesis (occurs at > 70℃ and at > 2 km, which is mediated by evolved formation waters) (Morad et al., 1990).

Based on the paragenetic relationships and the forming temperatures of the diagenetic minerals in sandstones as discussed above, and burial history curves, the relative diagenetic sequence of the Zhuhai sandstones is established and illustrated in Fig. 13.

The compaction and precipitation of calcite and dolomite are the dominant eogenetic processes in the Zhuhai sandstones. Moreover, framboidal pyrite and siderite are also demonstrated as the eogenetic, precompactional products in view of the filling relationships of these cements and primary pores between uncompacted framework grains (Figs 5f, 7g). Compaction extends throughout subsequent mesogenetic phases. Feldspar dissolution is one of the major mesogenetic processes experienced by the Zhuhai sandstones, and is closely accompanied by diagenetic by-products such as clay and quartz cements (Figs 7c, d; Giles and de Boer, 1990). The relative sequence in mesogenesis is concluded to be (1) feldspar dissolution, (2) kaolinite precipitation, (3) Qa1, (4) ferroan calcite, (5) feldspar dissolution, (6) illitization, (7) Qa2, and (8) ankerite, albite, and nodular pyrite precipitation (Figs 5, 7).

The hydrocarbon inclusions are pervasively developed and are closely associated with the coeval aqueous inclusions in quartz microfractures of the Zhuhai sandstones (Fig. 10a). The Th of the coeval aqueous inclusion is regarded as the closest equivalent to the trapping temperature of the coexisting hydrocarbon inclusions, as previously stated, which ranges from 94.3℃ to 146℃. This result accords with the previous detailed work of

Table 2. Isotopic composition and precipitation temperature of carbonate cements. Cc = calcite; Do = dolomite; Fc = ferroan calcite; An = ankerite

Well	Depth/m	Carbonte	$\delta^{13}C_{VPDB}$/‰	$\delta^{18}O_{VPDB}$/‰	Precipitation temperature/℃		
					$\delta^{18}O_{SMOW}$=−5 /‰	$\delta^{18}O_{SMOW}$=−2 /‰	$\delta^{18}O_{SMOW}$=0 /‰
LW4-1	1 519.8	Cc	0.97	−8.62	31	–	–
LW4-1	1 559.8	Cc	1.58	−9.92	38	–	–
LW1-1	1 657.64	Cc	2.51	−9.73	37	–	–
LW1-1	1 657.64	Cc	1.43	−10.44	41	–	–
LW1-1	1 708.25	Cc	0.11	−9.59	36	–	–
LW1-1	2 027.25	Cc	−0.30	−8.28	29	–	–
LW1-2	2 609.1	Cc	1.23	−11.27	45	–	–
LW4-1	1 514.8	Do	1.56	−8.75	61	–	–
LW1-1	1 671.5	Do	0.12	−10.31	72	–	–
LW1-1	1 713.5	Do	0.35	−9.49	66	–	–
LW1-1	2 026.5	Do	−0.76	−8.49	59	–	–
LW1-1	2 037.5	Do	2.12	−11.24	80	–	–
LW1-1	2 037.5	Do	1.44	−10.76	76	–	–
LW1-2	2 577.0	Do	1.54	−9.67	68	–	–
LW1-2	2 577.0	Do	0.73	−10.31	72	–	–
LW3-1	1 861.5	Fc	−7.48	−13.67	60	79	94
LW1-1	2 026.5	Fc	−11.96	−15.43	71	92	108
LW1-1	2 563.5	Fc	−24.42	−16.63	79	101	118
LW1-1	2 563.5	Fc	−13.87	−15.74	73	94	110
LW1-2	2 609.1	Fc	−10.72	−14.20	63	83	98
LW1-2	2 824.8	Fc	−4.19	−13.92	61	81	95
LW4-1	1 559.8	An	−7.53	−14.58	88	114	137
LW1-1	1 658.0	An	−7.72	−14.13	85	110	132
LW1-1	2 026.5	An	−4.48	−12.06	71	92	109
LW1-1	2 033.39	An	−2.47	−15.27	94	121	142
LW1-1	2 045.0	An	−1.02	−17.22	111	142	167
LW1-2	2 563.5	An	−3.36	−13.55	81	105	123
LW1-2	2 701.5	An	−2.65	−15.46	96	123	136
LW1-2	2 702.5	An	−7.25	−14.26	86	111	131
LW2-1	2 997.5	An	−6.51	−18.05	119	152	179

Note: "–" indicates no data.

Mi et al. (2019), which showed that two periods of hydrocarbon accumulation occurring respectively at 13.1–7.3 Ma and 5.5–0 Ma (Fig. 13) exist in the study area. The first period of hydrocarbon charge postdated the dissolution of feldspar, and antedated or was synchronous with the precipitation of mesogenetic ferroan calcite. The second period postdated the late ankerite cementation. Parts of reservoirs, it should be noted, especially the thin beds or the marginal parts of thick beds (<1 m away from the contact), were rich in early calcite and dolomite cements during eogenesis, even filled all the intergranular spaces and became tight reservoirs, and then hardly any other diagenetic alteration occurred.

5.2 *Source of quartz cements*

A much-debated question for quartz cements is whether there are external or internal sources of silica within given sandstones (Bjørlykke, 2014). External sources include deep fluid migration, adjacent mudstones and so on, which are revealed as sources in open geochemical systems (Thyne, 2001; Day-Stirrat et al., 2010). The main limitation with external silica sources, however, is the difficulty of long distance and massive transfer due to formation fluid with limited flow and low silica solubility (Bjørlykke and Jahren, 2012). By contrast, internal silica sources, including biogenic silica, feldspar and clay alteration reactions, quartz grain dissolution, and unstable volcanic rock fragments, are more convincing in most situations (Bjørlykke, 2014).

It can be inferred from the Th distribution (Table 1) that quartz cement (as overgrowth) was almost continuous growth (Walderhaug, 2000). The formation temperature range of the Qa1(77.5℃ to 107.9℃) is matched with the dominant temperature zones of organic acid production (Surdam Ronald et al., 1989). On the other hand, the content of quartz cement is positively associated with feldspar dissolution (Figs 6a, c). The feldspar alteration by organic acid must be a significant silica source for Qa1 (Worden and Morad, 2000). As mentioned above, a considerable amount of kaolinite exists above 2 000 m (temperature <100℃), and the rapid and mass transformation of kaolinite to illite occurs in sandstones below 2 000 m, especially between the depths of 2 200 m and 2 500 m (temperature varying from 100℃ to 120℃). The formation temperature range of the Qa2 (104.5℃ to 125℃) is coinciding with the optimal temperature zones of the illitization of kaolinite. It therefore seems that the illitization of kaolinite play an important role for Qa2 in the study area (Morad et al., 1990). The prismatic euhedral quartz crystals commonly precipitate within intergranular pores, but are always accompanied by detrital quartz grains covered by clay minerals. A possible reason for this phenomenon is that there is no place for the nucleation on the detrital quartz surface (Worden and Morad, 2000).

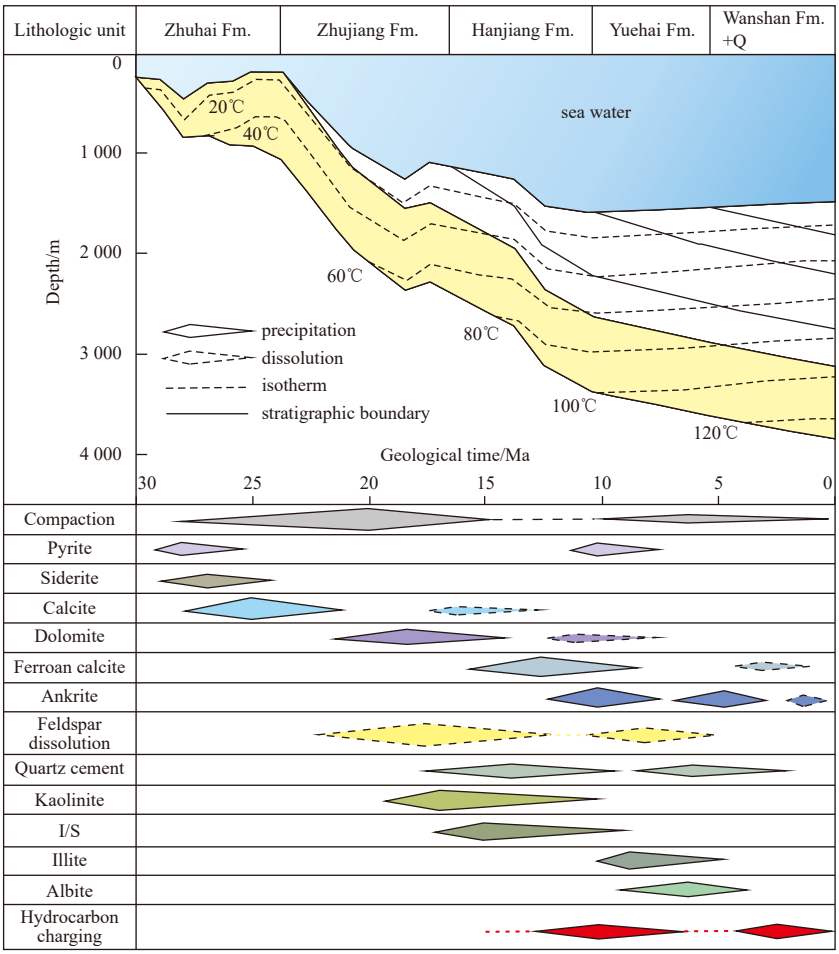

Fig. 13. Burial, thermal, and diagenetic history of the Zhuhai sandstones.

In addition, the point and linear contact between detrital minerals indicates that minimal pressure dissolution has occurred in the Zhuhai sandstones, suggesting the potentially limited significance of pressure dissolution for quartz overgrowth.

5.3 *Source of carbonate cements*

Several possible origins have been established for the components of carbonate cements, including internal (e.g., biogenic fragments or detrital grains), external (from adjacent mudstones), or mixed sources (Gier et al., 2008). According to the latitudinal gradient of $\delta^{18}O$ value, $\delta^{18}O_{SMOW}$ value of sedimentary water of the Baiyun Sag can be evaluated to –5‰ (range from 0‰ to –10‰), for the 20° N paleolatitude of the Sag (Rozanski et al., 1993). This could represent the $\delta^{18}O_{SMOW}$ value of early pore-fluids. According to the fractionation equations of the oxygen isotope for calcite-water and dolomite-water (Kim and O'Neil 1997; Schmidt et al., 2005), calculated formation temperatures are between 29℃ and 45℃ for calcite and between 59℃ and 80℃ for dolomite (Table 2).

The $\delta^{13}C$ value is a useful indicator to investigate the sources of carbonate cements (dos Anjos et al., 2000; Woo and Khim, 2006; El-Khatri et al., 2015). The interbedded shelf mudstones contain a considerable amount of organic matter (TOC values range from 0.66% to 1.47%, average 1.08%) (Li et al., 2011). The bicarbonate species related to microbial methanogenesis of organic matter ($\delta^{13}C$ up to +8‰) might provide important source for early formed carbonate. This can be supported by the relative positive $\delta^{13}C$ values (–0.76‰ to +2.51‰) of these cements (Table 2) (Whiticar et al., 1986). In addition, the mudstones in the Zhuhai Formation are high in detrital carbonate grains (over 15%) (Zhu et al., 2008). These minerals have $\delta^{13}C$ values that vary from 0‰ to +5.9‰ (Zhu et al., 2008). The dissolution of these detrital carbonate can thus be another carbon source (Zhu et al., 2009). Meanwhile, the Ca^{2+} and Mg^{2+} ions dissolved in the mudstone were probably transported to sandstone as well.

It is a widely held view that the $\delta^{18}O$ value becomes enhanced with the increase in temperature of pore-fluids, due to isotopically modification by feldspar alteration and a series of diagenetic actions (dos Anjos et al., 2000; Fayek et al., 2001). $\delta^{18}O_{SMOW}$ values were assumed to be –5‰, –2‰, and 0 for the pore fluid that late carbonate was precipitated in it (dos Anjos et al., 2000). Using a $\delta^{18}O_{SMOW}$ value of –2‰, with the fractionation equation of oxygen isotope for calcite-water and dolomite-water (Kim and O'Neil, 1997; Horita, 2014), precipitation temperatures of ferroan calcite can be calculated as 79–101℃, and 91–152℃ for ankerite (Table 2). The measured Th of fluid inclusions in ankerite (113.7℃, 124.3℃, Table 1) are both within the calculated results of ankerite (Table 1). The assumption of a $\delta^{18}O_{SMOW}$ value of -2‰ is acceptable. In addition, the illitization of smectite (60 – 100℃) in the mudstones is slightly prior to the precipitation of ferroan calcite (Boles and Franks, 1979), which can release Ca^{2+}, Fe^{3+}, Mg^{2+}, and silica for the ferroan calcite in sandstones (Curtis, 1978; Wang et al., 2016). This inference is also supported by the high content of carbonate cements at both sides of the sand-

stone-mudstone contacts (Fig. 6).

The relative negative $\delta^{13}C$ values (–24‰ to –1‰) of the ferroan calcite suggest an organic source from adjacent mudstones ($\delta^{13}C_{VPDB}$ from –25‰ to –10‰) (Table 2) (Curtis, 1978). Moreover, plenty of organic CO_2 derived from adjacent mudstones can dissolve some early-formed carbonate (Dutton, 2008), which could be demonstrated by the non-ferroan carbonate replaced and engulfed by ferroan carbonate. Thus, the $\delta^{13}C_{VPDB}$ values (–24‰ to –1‰) probably suggest there is a mixed carbon source of organic CO_2 and inorganic carbonate. In addition, ankerite cements have higher $\delta^{13}C$ values than ferroan calcite and they are formed at significantly high temperatures, thus indicating another origin from CO_2 contained deep fluid. The $\delta^{13}C$ values of the hydrothermal fluid from the deep are about –5 ‰ ± 2 ‰, and its generally positive $\delta^{18}O$ values range from +5.0‰ to +7.0‰ (Friedman and O'Neil, 1977). The uptrend of $\delta^{13}C$ values of ankerite and the enrichment of $\delta^{18}O$ values of pore waters with increasing temperature may be related to the uprising and intrusion of hydrothermal fluid from the deep to sandstones.

5.4 *Controls on reservoir quality*

It is well known that present-day reservoir quality is controlled by initial depositional attributes, which profound control the textural and mineralogical composition of the sediments, as well as pore fluid composition (pH, Eh), and subsequent diagenetic modifications, including compaction, location of diagenetic cements, and the generation of secondary porosity (Bjørlykke and Jahren, 2012; Kassem et al., 2022).

5.4.1 *Depositional controls on reservoir quality*

Texture (grain size and sorting) and composition determine the initial intergranular volume (IGV) of the sediments (dos Anjos et al., 2000; El-Khatri et al., 2015). The porosity and permeability correlate closely with sorting and the grain size since compaction is very sensitive to texture variation (Bjørlykke and Jahren, 2012; Bjørlykke, 2014).

Statistics show that the porosity increases as particle sizes increase, as shown in Fig. 14. The high-quality reservoirs correspond to the sandstone have a grain size larger than 0.3 mm (Fig. 14). The porosity tends to be higher in the coarser-grained sandstones as the pores between the larger grains could be filled with finer grains (Walderhaug et al., 2012), while relatively low porosities could be observed in some coarser-grained sandstones with strong carbonate cementation (Fig. 14). For Zhuhai reservoirs, the more poorly sorted a sediment is, the lower its intergranular volume and porosity. This is due to a much lower initial porosity and/or a more tightly compacted in the poorly sorted samples, which contain more silt and clay (Bjørlykke, 2014). Reservoir quality is better as the particle size increases and sorting improves.

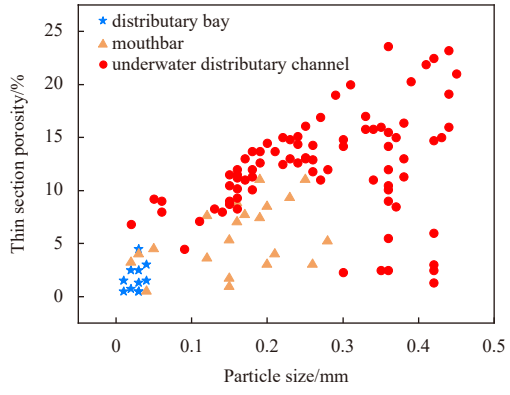

Fig. 14. Relationship between the porosity and particle size of different sedimentary micro-facies.

The grain composition can severely impact the reservoir quality of sandstones by conditioning the diagenesis pathway. Large differences in IGV (up to 10%–15%) have little to do with depth (Fig. 15a), but are more related to the content of original rock grains. Reservoirs with a higher content of quartz grains maintain a larger IGV, indicating higher degrees of mechanical stability and resistance to compression of the rigid quartz grains (Fig. 15b). The negative correlation between the IGV and the ductile grains, such as unstable rock fragments and chemically deformed feldspar grains, further suggests the significant influence of original rock grain composition on the IGV (Figs 15c and d).

These findings suggest that, in general, the reservoir quality is sedimentary selective. As can be seen from Fig. 14, the reservoir quality is highest in thick, underwater distributary channel facies, which are characterized by coarser-grained, better sorting, particle-support nature, as well as away from sandstone-mudstone contact. Distributary bay facies, which are characterized by lower energy, finer-grained, matrix-support nature, have the poorest porosity and permeability due to low initial porosity and extensive compaction (Fig. 14). The relatively low porosities in both underwater distributary channel and mouth bar facies typically occur at or near sandstone-mudstone contact which are characterized by tightly carbonate cementation. This resulted in significant porosity reduction during diagenesis (Figs 5a, 6a).

5.4.2 *Diagenetic controls on reservoir quality*

The porosity and permeability versus depth show that compaction, initiated immediately after deposition and throughout the entire burial process, can destroy the primary pore volume severely (Stroker et al., 2013). Samples without extensive eogenetic cement suggested that the deterioration of porosity was mainly due to compaction. A plot of IGV versus total intergranular cement and pseudomatrix (assuming that the sandstones had an initial porosity of 40% using tables from Lundegard (1992) indicates that compaction constituted about 32.25%–74.75% (average 54.6%) of the total pore volume loss during burial (Fig. 16).

Cementation is also a major factor which influences reservoir property in the studied sandstones, especially at local scales such as within a single sand body (Kassem et al., 2022). As demonstrated above, carbonate mineral, the most abundant pore-occluding cement type, is mainly formed from external mass sources (adjacent muddy source rocks). The relationship between carbonate cements and reservoir properties is highlighted in Fig. 17. For samples taken from margin sandstones within 1.0 m of the sandstone-mudstone contact, the content of carbonate cements is generally greater than 15%, and the porosity is lower than 10% (Fig. 17). Consequently, thin sandstone layers ($\leqslant$2 m) always show poor reservoir properties due to strong carbonate cementation. For thicker sandstone bodies (>2 m), the reservoir properties rise steadily along with successive increases in the distance to the contact.

Effective secondary porosity can be loosely defined as the difference between feldspar dissolution porosity and pore-filling by-products (mainly authigenic quartz and clay) (Fig. 18; Giles and de Boer, 1990). It ranges from –1.9% to 1.6% via quantitative calculation of the studied sandstone (Fig. 18d). The calculated negative value implies that feldspar dissolution did not cause any significant increment of porosity. In view of 25%–50% microporosity of clay minerals, the increment of porosity can be calcu-

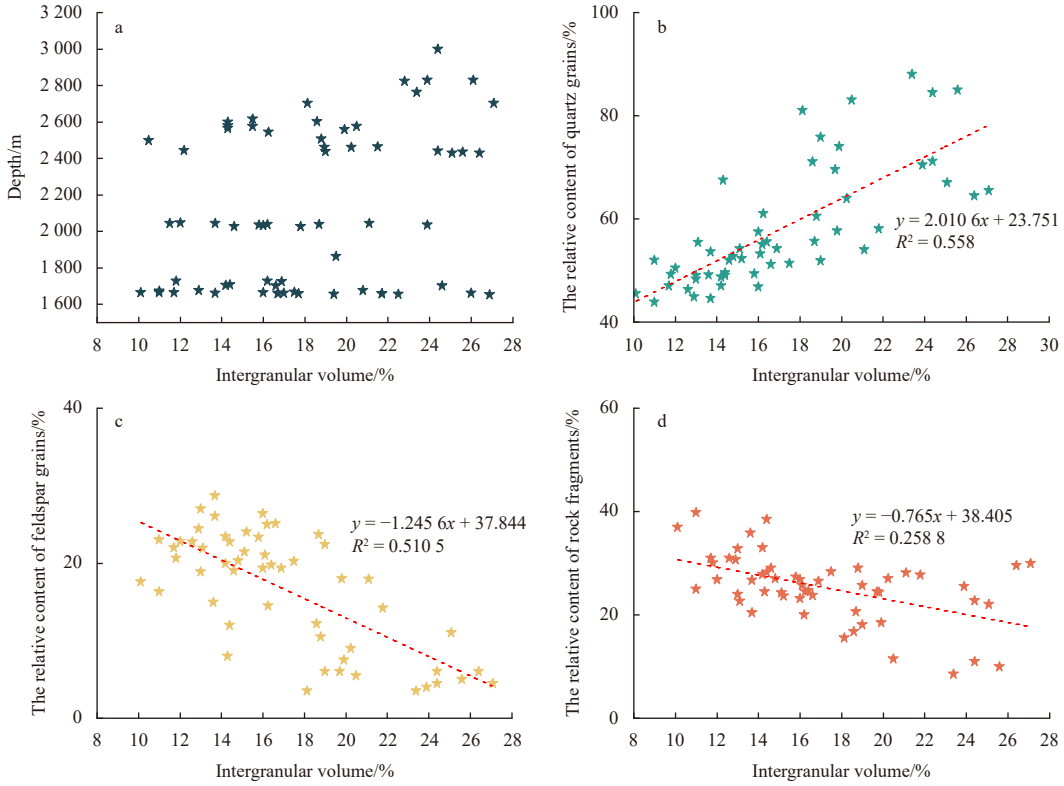

Fig. 15. Relationships between depth, composition of detrital grains and IGV in the Zhuhai sandstones.

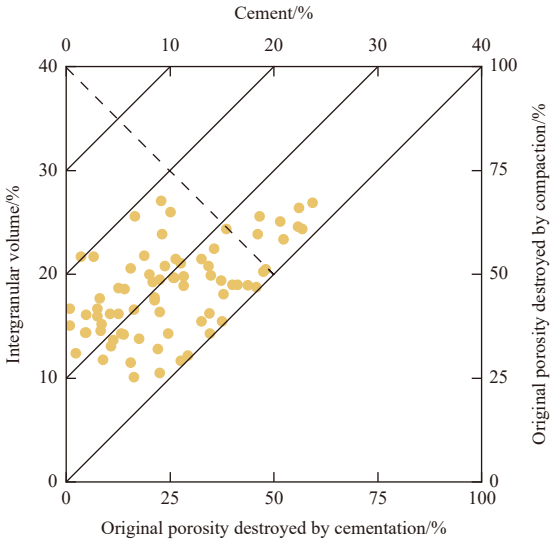

Fig. 16. Plot of IGV versus volume of cement in the Zhuhai sandstones (modified from Lundegard, 1992).

lated by feldspar dissolution porosity minus 62.5% clay minus authigenic quartz (Nadeau and Hurst, 1991; Yuan et al., 2015). And then, the absolute increment of porosity ranges from –0.66% to 1.18% (Fig. 18e), which suggests a relatively closed diagenetic system (Taylor et al., 2010). Although the reservoir porosity shows little or no net increment, primary macropores were substituted by micropores occurring between authigenic clay crystals and within dissolved residual feldspars (Nadeau and Hurst, 1991). The pore connectivity relatively decreases owing to the precipitation of clay and quartz cements. As a result, the permeability of the reservoirs is degenerative to some degree. Especially for the deep buried sandstone (>2 000 m) that experienced relatively strong compaction, the permeability was significantly reduced due to pore-throat plugging by authigenic quartz and clay (mostly illite) (Figs 8, 9).

In summary, the depositional parameters such as grain size and sorting had critical controls on diagenetic modifications, which in turn determined the reservoir quality of the Zhuhai reservoirs. To conclude, good quality reservoirs in Zhuhai sandstones are characterized as medium-grained lying in the central parts of thick underwater distributary channel sandbodies (>2 m) with a high content of detrital quartz but low cements, such as carbonates and clay minerals. The findings will improve the predictive capabilities of high-quality reservoirs in the Baiyun Sag, and have wide application for the pre-drill prediction of anomalous high porosity reservoirs with geologically similar conditions.

6 Conclusions

This study has provided an insight into the diagenesis and its impact on the reservoir quality of the Oligocene Zhuhai sandstones in the Baiyun Sag. The findings may provide an analogue for the study of reservoir quality evaluation and prediction of clastic reservoirs in other basins. On the basis of detailed analyses of petrology, mineralogy, carbon and oxygen isotope ratios, and fluid inclusion homogenization temperatures, this study has demonstrated the following:

(1) The Zhuhai sandstones are mainly feldspathic litharenites and lithic arkoses, which are marked by abundant volcanic rock fragments, with a fine to medium grain size and moderate to good sorting.

(2) The reservoir properties are of significant heterogeneity, with porosity ranging from 0.2% to 36.1% and permeability from 0.016 $\times 10^{-3}$ μm² to 4 301.45 $\times 10^{-3}$ μm². The visual pores are dominated by primary intergranular pores and decrease with the

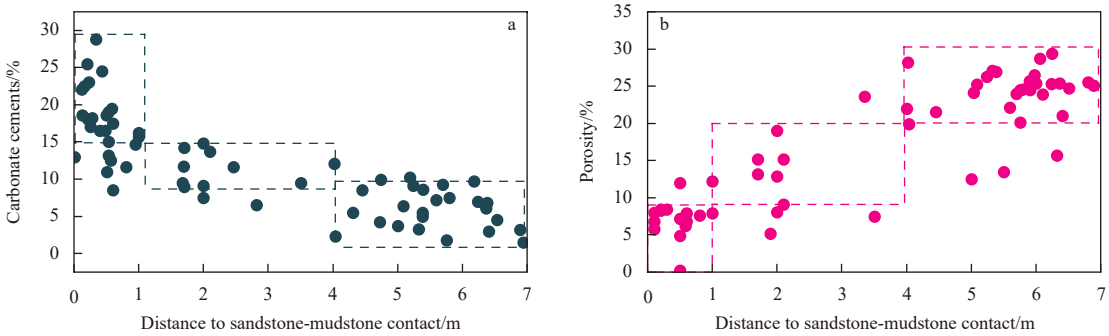

Fig. 17. Relationships between carbonate contents (%) and the distance to sandstone-mudstone contact (a). Relationships between porosity (%) and the distance to sandstone-mudstone contact (b).

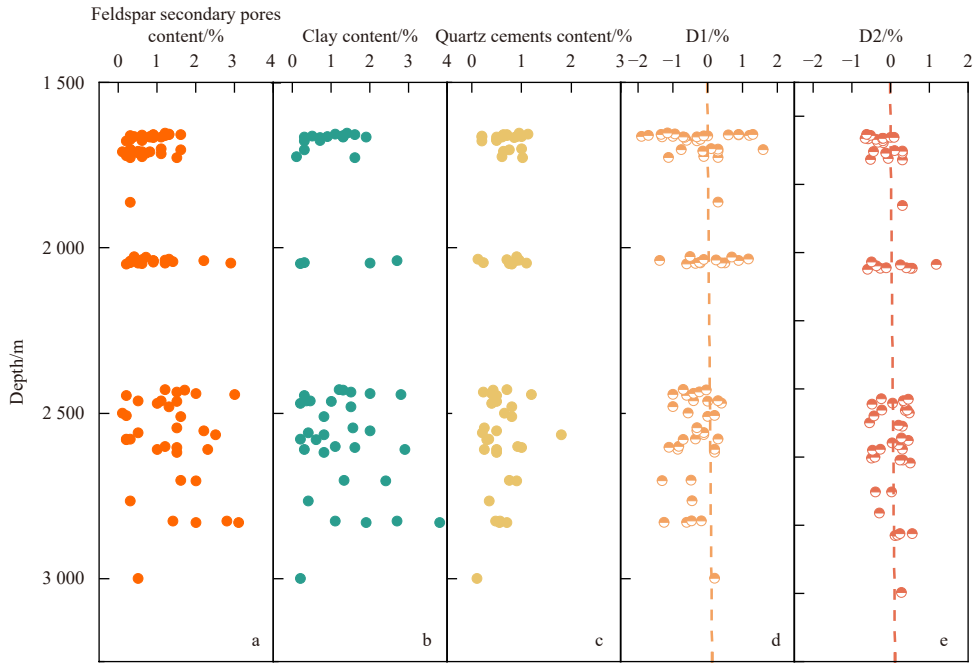

Fig. 18. The vertical distribution of the content of diagenetic products (a–c), effective secondary porosity (D1, d) and increment of porosity (D2, e).

burial depth, while the relative contents of feldspar secondary pores show an increasing trend.

(3) Eogenesis includes compaction, cementation of calcite, dolomite, siderite and framboidal pyrite. Mesogenesis includes further compaction, feldspar dissolution, precipitation of ferrocalcite and ankerite, quartz cements, formation of kaolin and its illitization, precipitation of albite and nodular pyrite, as well as hydrocarbon charge.

(4) Feldspar dissolution and illitization of kaolinite provide significant internal sources of silica for the quartz cementation. Carbonate cementation mainly stems from external sources related to interbedded mudstones and deep fluid. Specifically, they are mainly from microbial methanogenesis in eogenesis, from organic CO_2 in mesogenesis, and from hydrothermal fluid for late ankerite.

(5) Compaction is the predominant factor in reducing the total porosity, followed by carbonate cementation that leads to strong heterogeneity within one sandstone bed. Feldspar dissolution barely changes the porosity but significantly reduces the permeability due to concomitant quartz and clay cementation.

(6) By linking diagenesis to sedimentary micro-facies, the high-quality reservoirs can be concluded as medium-grained sandstones lying in the central parts of thick underwater distributary channel sandbodies (>2 m) with a high content of detrital quartz but low cements.

References

Bjørlykke K. 2014. Relationships between depositional environments, burial history and rock properties. Some principal aspects of diagenetic process in sedimentary basins. Sedimentary Geology, 301: 1–14, doi: 10.1016/j.sedgeo.2013.12.002

Bjørlykke K, Jahren J. 2012. Open or closed geochemical systems during diagenesis in sedimentary basins: constraints on mass transfer during diagenesis and the prediction of porosity in sandstone and carbonate reservoirs. AAPG Bulletin, 96(12): 2193–2214, doi: 10.1306/04301211139

Boles J R, Franks S G. 1979. Clay diagenesis in Wilcox sandstones of Southwest Texas: implications of smectite diagenesis on sandstone cementation. Journal of Sedimentary Research, 49(1): 55–70

Coplen T B, Kendall C, Hopple J. 1983. Comparison of stable isotope reference samples. Nature, 302(5905): 236–238, doi: 10.1038/

302236a0
Curtis C D. 1978. Possible links between sandstone diagenesis and depth-related geochemical reactions occurring in enclosing mudstones. Journal of the Geological Society, 135(1): 107–117, doi: 10.1144/gsjgs.135.1.0107
Day-Stirrat R J, Milliken K L, Dutton S P, et al. 2010. Open-system chemical behavior in deep Wilcox Group mudstones, Texas Gulf Coast, USA. Marine and Petroleum Geology, 27(9): 1804–1818, doi: 10.1016/j.marpetgeo.2010.08.006
dos Anjos S M C, De Ros L F, de Souza R S, et al. 2000. Depositional and diagenetic controls on the reservoir quality of lower cretaceous Pendencia Sandstones, Potiguar Rift basin, Brazil. AAPG Bulletin, 84(11): 1719–1742
Du Guichao, Su Long, Chen Guojun, et al. 2019. Carbonate cements and its effect on reservoir property of shallow marine sandstones of Zhuhai Formation in Panyu low-uplift, Pearl River Mouth Basin. Lithologic Reservoirs (in Chinese), 31(3): 10–19
Dutton S P. 2008. Calcite cement in Permian deep-water sandstones, Delaware Basin, west Texas: origin, distribution, and effect on reservoir properties. AAPG Bulletin, 92(6): 765–787, doi: 10.1306/01280807107
El-Khatri F, El-Ghali M A K, Mansurbeg H, et al. 2015. Diagenetic alterations and reservoir quality evolution of lower cretaceous fluvial sandstones: Nubian Formation, Sirt Basin, North-Central Libya. Journal of Petroleum Geology, 38(2): 217–239, doi: 10.1111/jpg.12607
Fayek M, Harrison T M, Grove M, et al. 2001. In situ stable isotopic evidence for protracted and complex carbonate cementation in a petroleum reservoir, north Coles levee, San Joaquin Basin, California, U. S. A. Journal of Sedimentary Research, 71(3): 444–458, doi: 10.1306/2DC40954-0E47-11D7-8643000102C1865D
Folk R L. 1968. Petrology of Sedimentary Rocks. Austin: Hemphill Publishing Company
Friedman I, O'Neil J R. 1977. Compilation of stable isotope fractionation factors of geochemical interest. US Geological Survey Professional Paper, 440-KK
Gier S, Worden R H, Johns W D, et al. 2008. Diagenesis and reservoir quality of Miocene sandstones in the Vienna Basin, Austria. Marine and Petroleum Geology, 25(8): 681–695, doi: 10.1016/j.marpetgeo.2008.06.001
Giles M R, de Boer R B. 1990. Origin and significance of redistributional secondary porosity. Marine and Petroleum Geology, 7(4): 378–397, doi: 10.1016/0264-8172(90)90016-A
Horita J. 2014. Oxygen and carbon isotope fractionation in the system dolomite-water-CO_2 to elevated temperatures. Geochimica et Cosmochimica Acta, 129: 111–124, doi: 10.1016/j.gca.2013.12.027
Kassem A A, Hussein W S, Radwan A E, et al. 2021. Petrographic and diagenetic study of siliciclastic Jurassic sediments from the northeastern margin of Africa: implication for reservoir quality. Journal of Petroleum Science and Engineering, 200: 108340, doi: 10.1016/j.petrol.2020.108340
Kassem A A, Osman O A, Nabawy B S, et al. 2022. Microfacies analysis and reservoir discrimination of channelized carbonate platform systems: an example from the Turonian Wata Formation, Gulf of Suez, Egypt. Journal of Petroleum Science and Engineering, 212: 110272, doi: 10.1016/j.petrol.2022.110272
Kim S T, O'Neil J R. 1997. Equilibrium and nonequilibrium oxygen isotope effects in synthetic carbonates. Geochimica et Cosmochimica Acta, 61(16): 3461–3475, doi: 10.1016/S0016-7037(97)00169-5
Lei Chuan, Luo Jinglan, Pang Xiong, et al. 2018. Impact of temperature and geothermal gradient on sandstone reservoir quality: the Baiyun Sag in the Pearl River Mouth Basin study case (northern South China Sea). Minerals, 8(10): 452, doi: 10.3390/min8100452
Li Chi, Luo Jinglan, Fan Caiwei, et al. 2021. Impact of high thermal setting and fluid activities on sandstone compaction: a case study of the Baiyun Sag in the Pearl River mouth basin (Northern South China Sea). Geofluids, 2021: 6658729
Li Youchuan, Mi Lijun, Zhang Gongcheng, et al. 2011. The formation and distribution of source rocks for deep water area in the northern of South China Sea. Acta Sedimentologica Sinica (in Chinese), 29(5): 970–979
Liao Jihua, Wu Keqiang, Er Chuang. 2022. Deep reservoir characteristics and effective reservoir control factors in Baiyun Sag of Pearl River Mouth Basin. Earth Science (in Chinese), 47(7): 2454–2467
Lundegard P D. 1992. Sandstone porosity loss — a "big picture" view of the importance of compaction. Journal of Sedimentary Research, 62(2): 250–260, doi: 10.1306/D42678D4-2B26-11D7-8648000102C1865D
Mangi H N, Chi Ruan, Yan Detian, et al. 2022. The ungrind and grinded effects on the pore geometry and adsorption mechanism of the coal particles. Journal of Natural Gas Science and Engineering, 100: 104463, doi: 10.1016/j.jngse.2022.104463
Mansurbeg H, Morad S, Salem A, et al. 2008. Diagenesis and reservoir quality evolution of palaeocene deep-water, marine sandstones, the Shetland-Faroes Basin, British continental shelf. Marine and Petroleum Geology, 25(6): 514–543, doi: 10.1016/j.marpetgeo.2007.07.012
Mi Lijun, He Min, Zhai Puqiang, et al. 2019. Integrated study on hydrocarbon types and accumulation periods of Baiyun sag, deep water area of Pearl River Mouth basin under the high heat flow background. China Offshore Oil and Gas (in Chinese), 31(1): 1–12
Mi Lijun, Liu Baojun, He Min, et al. 2016. Petroleum geology characteristics and exploration direction in Baiyun deep water area, northern continental margin of the South China Sea. China Offshore Oil and Gas (in Chinese), 28(2): 10–22
Moore D M, Reynolds R C Jr. 1997. X-Ray Diffraction and the Identification and Analysis of Clay Minerals. 2nd ed. Oxford: Oxford University Press, 378
Morad S, Al-Aasm I S, Ramseyer K, et al. 1990. Diagenesis of carbonate cements in Permo-Triassic sandstones from the Iberian Range, Spain: evidence from chemical composition and stable isotopes. Sedimentary Geology, 67(3–4): 281–295, doi: 10.1016/0037-0738(90)90039-V
Morley C K. 2016. Major unconformities/termination of extension events and associated surfaces in the South China Seas: review and implications for tectonic development. Journal of Asian Earth Sciences, 120: 62–86, doi: 10.1016/j.jseaes.2016.01.013
Muther T, Qureshi H A, Syed F I, et al. 2022. Unconventional hydrocarbon resources: geological statistics, petrophysical characterization, and field development strategies. Journal of Petroleum Exploration and Production Technology, 12(6): 1463–1488, doi: 10.1007/s13202-021-01404-x
Nadeau P H, Hurst A. 1991. Application of back-scattered electron microscopy to the quantification of clay mineral microporosity in sandstones. Journal of Sedimentary Research, 61(6): 921–925
Pang Xiong, Chen Changmin, Peng Dajun, et al. 2008. Basic geology of Baiyun deep-water area in the northern South China Sea. China Offshore Oil and Gas (in Chinese), 20(4): 215–222
Pang Xiongqi, Jia Chengzao, Wang Wenyang. 2015. Petroleum geology features and research developments of hydrocarbon accumulation in deep petroliferous basins. Petroleum Science, 12(1): 1–53, doi: 10.1007/s12182-015-0014-0
Rozanski K, Araguás-Araguás L, Gonfiantini R. 1993. Isotopic patterns in modern global precipitation. In: Swart P K, Lohmann K C, Mckenzie J, et al, eds. Climate Change in Continental Isotopic Records. Washington: American Geophysical Union, 1–36
Schmidt M, Xeflide S, Botz R, et al. 2005. Oxygen isotope fractionation during synthesis of CaMg-carbonate and implications for sedimentary dolomite formation. Geochimica et Cosmochimica Acta, 69(19): 4665–4674, doi: 10.1016/j.gca.2005.06.025
Shehata A A, Kassem A A, Brooks H L, et al. 2021. Facies analysis and sequence-stratigraphic control on reservoir architecture: example from mixed carbonate/siliciclastic sediments of Raha Formation, Gulf of Suez, Egypt. Marine and Petroleum Geology, 131: 105160, doi: 10.1016/j.marpetgeo.2021.105160
Stroker T M, Harris N B, Crawford Elliott W, et al. 2013. Diagenesis of

a tight gas sand reservoir: upper Cretaceous Mesaverde Group, Piceance Basin, Colorado. Marine and Petroleum Geology, 40: 48–68, doi: 10.1016/j.marpetgeo.2012.08.003

Surdam Ronald C, Crossey L J, Hagen E S, et al. 1989. Organic-inorganic interactions and sandstone diagenesis. AAPG Bulletin, 73(1): 1–23

Taylor T R, Giles M R, Hathon L A, et al. 2010. Sandstone diagenesis and reservoir quality prediction: models, myths, and reality. AAPG Bulletin, 94(8): 1093–1132, doi: 10.1306/04211009123

Thyne G. 2001. A model for diagenetic mass transfer between adjacent sandstone and shale. Marine and Petroleum Geology, 18(6): 743–755, doi: 10.1016/S0264-8172(01)00025-3

Tian Bing, Zheng Youwei, Zhao Junmei. 2022. Sedimentary facies and evolution of Oligocene Zhuhai Formation in Baiyun Sag, South China Sea. Fault-Block Oil & Gas Field (in Chinese), 29(6): 800–806,836

Walderhaug O. 2000. Modeling quartz cementation and porosity in Middle Jurassic Brent Group sandstones of the Kvitebjørn field, northern North Sea. AAPG Bulletin, 84(9): 1325–1339

Wang Jian, Cao Yingchang, Liu Keyu, et al. 2016. Pore fluid evolution, distribution and water-rock interactions of carbonate cements in red-bed sandstone reservoirs in the Dongying Depression, China. Marine and Petroleum Geology, 72: 279–294, doi: 10.1016/j.marpetgeo.2016.02.018

Wang Qi, Hao Lewei, Chen Gongcheng, et al. 2010. Forming mechanism of carbonate cements in siliciclastic sandstone of Zhuhai Formation in Baiyun Sag. Acta Petrolei Sinica (in Chinese), 31(4): 553–558,565

Wang Daifu, Luo Jinglan, Chen Shuhui, et al. 2017. Carbonate cementation and origin analysis of deep sandstone reservoirs in the Baiyun sag, Pearl River Mouth Basin. Acta Geologica Sinica (in Chinese), 91(9): 2079–2090

Wen Jing, Zhao Jingzhou, Li Jun, et al. 2022. Characteristics of mid-deep paleogene sandstone reservoirs in Baiyun Sag and controlling effect of dissolution on high-quality reservoirs. Special Oil & Gas Reservoirs (in Chinese), 29(6): 47–55

Whiticar M J, Faber E, Schoell M. 1986. Biogenic methane formation in marine and freshwater environments: CO_2 reduction *vs*. acetate fermentation-Isotope evidence. Geochimica et Cosmochimica Acta, 50(5): 693–709, doi: 10.1016/0016-7037(86)90346-7

Woo K S, Khim B K. 2006. Stable oxygen and carbon isotopes of carbonate concretions of the Miocene Yeonil Group in the Pohang Basin, Korea: types of concretions and formation condition. Sedimentary Geology, 183(1-2): 15–30, doi: 10.1016/j.sedgeo.2005.09.005

Worden R H, Morad S. 2000. Quartz cementation in oil field sandstones: a review of the key controversies. In: Worden R H, Morad S, eds. Quartz Cementation in Sandstones. Wiley-Blackwell: International Association of Sedimentologists, 1–20

Xie Xiaojun, Xiong Lianqiao, Bai Haiqiang, et al. 2022. Characteristics of favorable reservoir and its distribution prediction in middle-deep layers in Baiyun Sag, Pearl River Mouth Basin. Earth Science (in Chinese), 47(5): 1635–1651

Yuan Guanghui, Gluyas J, Cao Yingchang, et al. 2015. Diagenesis and reservoir quality evolution of the Eocene sandstones in the northern Dongying Sag, Bohai Bay Basin, East China. Marine and Petroleum Geology, 62: 77–89, doi: 10.1016/j.marpetgeo.2015.01.006

Zhou Wei, Gao Xianzhi, Wang Yingmin, et al. 2015. Seismic geomorphology and lithology of the early Miocene Pearl River Deepwater Fan System in the Pearl River Mouth Basin, northern South China Sea. Marine and Petroleum Geology, 68: 449–469, doi: 10.1016/j.marpetgeo.2015.09.006

Zhu Weilin, Huang Baojia, Mi Lijun, et al. 2009. Geochemistry, origin, and deep-water exploration potential of natural gases in the Pearl River Mouth and Qiongdongnan basins, South China Sea. AAPG Bulletin, 93(6): 741–761, doi: 10.1306/02170908099

Zhu Junzhang, Shi Hesheng, He Min, et al. 2008. Origins and geochemical characteristics of gases in LW3-1-1 well in the deep sea region of Baiyun Sag, Pearl River Mouth Basin. Natural Gas Geoscience (in Chinese), 19(2): 229–233